

Identifying the Active Site on Graphene Oxide Nanosheets for Ambient Electrocatalytic Nitrogen Reduction

Sini Wang, Jingjing Zhu, Yicheng Zhang, Qiangchun Liu, Guilin Chen,* and Xiangkai Kong*

Cite This: <https://dx.doi.org/10.1021/acs.inorgchem.0c01596>

Read Online

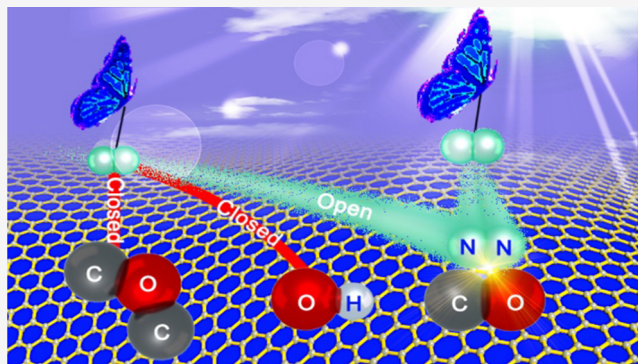
ACCESS |

Metrics & More

Article Recommendations

Supporting Information

ABSTRACT: Identifying the active sites on graphene oxide (GO) nanosheets is of great importance. In situ electroreduction at different potentials is applied to control the oxygenated groups on GO surfaces. Both experiments and theoretical calculations suggest the C=O group is critical for N₂ adsorption and activation, guaranteeing the ambient electrocatalytic N₂ reduction.



Ammonia (NH₃) has become the second-largest produced chemical around the world (170 million tons every year), as it is the basic sector of fertilizer, refrigerant, medication, dye, resin, and other important chemical feedstocks.¹ NH₃ possesses a large hydrogen content (17.7 wt %) and a high gravimetric energy density (3 kW h kg⁻¹), and it is technically ready for operation, thereby being regarded as an ideal energy carrier and a promising storage intermediate for renewable energy sources.² Currently, the industrial production of NH₃ highly relies on the Haber-Bosch process. However, this process requires high temperatures (550 °C) and elevated pressures (>200 atm) to accelerate the sluggish reaction kinetics, owing to the extremely stable and inert nitrogen molecules (941 kJ mol⁻¹) due to the strong triple bond.³ Meanwhile, this process takes fossil fuels as the precursor and generates significant CO₂ emission, and thus it will create serious environmental concerns.⁴ As a result, seeking a new and sustainable approach associated with efficient catalysts to favor the N₂ reduction at a low temperature and pressure remains an elusive challenge and is highly demanded.

Since the first attempt by Davy et al. in 1807, the electrochemical approach is demonstrated to offer the hope to synthesize NH₃ under mild conditions.⁵ Protons and electrons are directly used to facilitate the reduction of atmospheric N₂, which can be powered by renewable electricity.^{6,7} Intensive efforts are made in designing and preparing metal-based electrocatalysts for the nitrogen reduction reaction (NRR), including Ru,^{8,9} Au,^{10,11} Pd,¹² Mo,^{13,14} Fe,¹⁵ Cr,¹⁶ and Bi.² In addition, B₄C,¹⁷ boron nanosheets,¹⁸ black phosphorus nanosheets,¹⁹ B–N pairs,²⁰ and other metal-free materials have attracted much attention, not only because they are inexpensive but also because they are

attributed to their reducing environmental impact that can avoid metal ion release.^{21–25} Graphene is a classic metal-free material with unique properties, and appropriate surface functionalization can provide efficient sites for N₂ fixation;²⁶ recently, boron-doped graphene,²⁷ fluorographene,²⁸ and sulfur dots-graphene²⁹ have all exhibited a boosted performance for NRR.

The NH₃ synthesis from ambient N₂ involves six electron-coupled transfer steps, described as N₂ + 6H⁺ + 6e⁻ → 2NH₃.³⁰ An efficient catalyst is required to benefit the adsorption of N₂ on a surface, and it is followed by successive N≡N bond breaking and N–H bond formation, associated with consecutive proton hydrogenation. Generally, the chemisorption and sufficient activation of N₂ molecules is considered as the prerequisite for NRR. Therefore, the interactions between catalyst and N₂ as well as corresponding intermediates should be paid great efforts for the mechanism study. In this study, we envisioned graphene oxide (GO) nanosheets as the NRR catalyst. There are plenty of oxygenated groups, including OH, O–C–O, C=O, and COOH bonds on the surface. We made efforts to recognize and distinguish their effects in NRR. On the basis of experimental measurements and theoretical calculations, we

Received: May 31, 2020

suppose the C=O group takes the pivotal role in the ambient electrocatalytic N_2 reduction.

GO dispersion is dropped onto a clean carbon paper (CP) by the spin-coating method to form a uniform thin film covering the whole CP electrode. At first, its electrochemical behavior is studied by cyclic voltammetry (CV) using a three-electrode system in the 0.1 M Na_2SO_4 solution, with the raw GO material, a graphite rod, and Ag/AgCl as the working electrode, counter electrode, and reference electrode, respectively. In evidence, a significant reduction peak is clearly observed on GO at -0.67 V versus a reversible hydrogen electrode (RHE) (Figure 1a). Since there are abundant

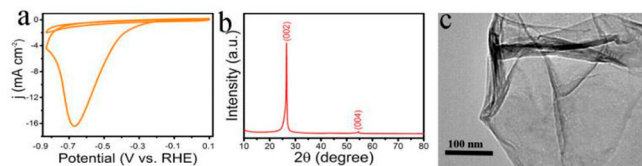


Figure 1. (a) CV curves of GO in the 0.1 M Na_2SO_4 solution. (b) XRD and (c) TEM image of ERGO-0.4.

oxygenated groups on the surface, this peak should be ascribed to the reduction of these oxygen-related species. In the second scanning cycle, this peak becomes much weaker and almost disappears, demonstrating the surface oxygenated groups can be easily and irreversibly removed.³¹ Of note, this electroreduction peak is quite broadened, with the half-peak width of ~ 0.2 V. This suggests these decorated groups can be reduced in control via applying appropriate potentials, and thus it offers the opportunity to study their individual roles in NRR. The in situ electroreduction is thereby performed at a constant potential in the range from -0.6 to -0.2 V for 100 s, and the obtained samples are denoted as ERGO-X, with X representing the specific applied reduction potential. As a typical example, ERGO-0.4 is studied in detail. Figure 1b presents its X-ray diffraction (XRD) pattern. There are no obvious diffraction peaks except for the CP signals at 26.6° and 54.5° , indicating the formation of an amorphous phase. A scanning electron microscopy (SEM) image is shown in Figure S1. A transmission electron microscopy (TEM) image demonstrates its thin sheetlike configuration, with some stacking and strips observed on surface (Figure 1c).

To examine the NRR performance on ERGO-0.4, we performed the electrochemical test using a two-compartment cell with a Nafion 211 membrane separating the anode and cathode chambers. The NRR activity is evaluated at potentials before the reduction current of oxygenated groups appearing. Figure 2a compares the linear sweep voltammetry (LSV) curves measured on ERGO-0.4 in the N_2 - and Ar-saturated 0.1 M Na_2SO_4 electrolyte, normally by the geometric area of CP electrodes. A lower recorded curve with a higher current density under the N_2 environment is discerned, indicating the occurrence of NH_3 generation from N_2 reduction. After 2 h of NRR electrocatalysis at specific potentials, the electrolyte is colored and withdrawn to analyze the obtained products by ultraviolet–visible (UV–vis) spectrophotometry.

The desired NH_3 product is determined by the indophenol blue method, and the byproduct N_2H_4 is investigated by the Watt and Chrisp method. The corresponding time-dependent current density curves exhibit relatively steady configuration as recorded in Figure 2b, implying ERGO-0.4 is chemically stable

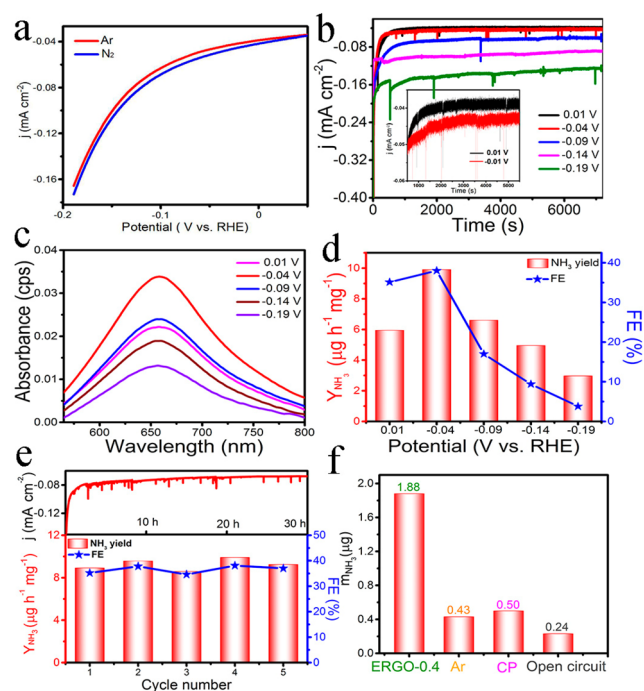


Figure 2. NRR performance on ERGO-0.4. (a) LSV curves in N_2 - and Ar-saturated electrolyte. (b) Time-dependent current density curves at different potentials. (c) UV–Vis spectra with indophenol indicator after the NRR reaction at different potentials. (d) Yield of NH_3 and corresponding FEs. (e) Long-time operation and repeated NRR performance measurement at -0.04 V. (f) m_{NH_3} under a series of conditions.

during the ambient N_2 reduction. Figure 2c shows the collected absorption spectra of the electrolytes stained with the indophenol indicator after electrolysis for another 2 h.² On the basis of calibration (Figures S2 and S3), ERGO-0.4 delivers the highest NH_3 yield of $9.9 \mu g h^{-1} mg^{-1}$ at -0.04 V with the corresponding faradaic efficiency (FE) of 38.1% (Figure 2d). Although this activity is inferior to some reported metal-based materials, the applied potential here is extremely small and thus leads to a high FE value. In the meantime, its capability is comparable to the defect-rich fluorographene nanosheets³⁰ and also some recent reported NRR electrocatalysts [Table S1]. Of note, there is no N_2H_4 detected after the reaction, confirming the excellent selectivity of ERGO-0.4 for NH_3 synthesis (Figure S4). Furthermore, the stability is evaluated by a long-time NRR measurement with the current density versus time ($i-t$) curve as shown in Figure 2e, where a stable current density response without obvious fluctuation is observed for 30 h. Recycling experiments are also conducted, and the yield shows minor change during five consecutive cycles, implying its superior long-time operation behavior (Figure 2e).

Control experiments are executed to examine the interference from environmental contamination and verify the N source of the produced NH_3 . A bare CP electrode shows much low NH_3 concentration in the N_2 saturated electrolyte at the same potential for 2 h (Figure 2f). In addition, ERGO-0.4 in the N_2 -saturated medium at the open-circuit potential also presents no apparent NH_3 generation. Besides, when N_2 dissolved in the electrolyte is exhausted by an Ar purge, there is still no obvious NH_3 signal measured. Their absorption spectra are collected in Figure S5. The minor detected NH_3 absorbance can be attributed to the trace amount of NH_3 from

air contamination.² The ¹H NMR spectra demonstrate only ¹⁵NH₄ was observed when using ¹⁵N₂ as the feeding gas (Figure S6). The static experiment with an intermittent N₂ supply reveals the high dependence of the reduction current density on N₂ (Figure S7). Figures S8 and S9 demonstrate the highly linear relationship between the ammonia production and reaction time. These results convincingly confirm the NH₃ is produced from N₂ electrochemical reduction on ERGO-0.4 in the ambient environment.

To distinguish the effects of an individual oxygenated functional group on N₂ reduction and identify the actual sites for NH₃ generation, we used the chronoamperometry strategy at different potentials to prepare ERGO with controllable oxygenated groups. Figure 3a shows the original peak intensity

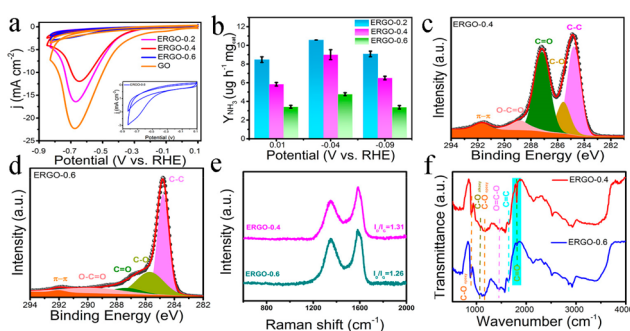


Figure 3. (a) CV curves on a series of ERGO materials. (inset) The magnification of CV curves measured on ERGO-0.6. (b) NH₃ yield comparison between ERGO-0.2 (three times), ERGO-0.4 (five times), and ERGO-0.6 (three times). XPS spectra of C 1s for (c) ERGO-0.4 and (d) ERGO-0.6. (e) Raman and (f) FTIR spectra for ERGO-0.4 and ERGO-0.6.

will become smaller when a larger reduction potential is applied. As the potential increases to -0.6 V, this reduction peak gets flat and almost disappears (inset in Figure 3a). The electrochemically active surface area (ECSA) is evaluated by running the CV at different scanning rates in the double-layer potential region. Figure S10 illustrates that ERGO-0.6 possesses a much smaller charging/discharging capacitance when compared with ERGO-0.4, which confirms the realization of a controllable and partial reduction of the surface oxygen species. The NRR performance on ERGO-0.2 and ERGO-0.6 are summarized in Figures S11 and S12. Figure 3b compares the NH₃ yields of ERGO-0.2, -0.4, and -0.6, all of which are collected from at least three individual measurements based on separated electrodes. ERGO-0.4 attains a comparable performance as that of ERGO-0.2, while ERGO-0.6 exhibits significantly reduced NRR activity. Electrochemical impedance spectroscopy (EIS) data present an apparently smaller semicircle on ERGO-0.4 than on ERGO-0.6, confirming the significant activity decrease from -0.4 to -0.6 V reduction (Figure S13). These results indicate the changes in surface structure and chemical environment from -0.4 to -0.6 V reduction are essential to determine the NRR activity.

X-ray photoelectron spectroscopy (XPS) measurement is further conducted to investigate the chemical composition change and environment variation during the potential-dependent electroreduction process. For the C 1s spectra as shown in Figure 3c,d and Figure S14a, there are four deconvoluted peaks located at 284.8, 285.6, 287.2, and 288.8

eV, which are attributed to the C–C, C–O, C=O, and O–C=O bonds, respectively.³² The C=O/C–C ratio decreases from 1.18 to 1.08 and further to 0.22 when the reduction potential changes from -0.2 to -0.4 and -0.6 V. Correspondingly, the O/C atomic ratio decreases from 0.43 to 0.40 and further to 0.18. The relative O–H peak intensity gets smaller as the applied potential turns from -0.2 to -0.4 V (Figures S14b and S15). Besides, the O=C peak of the O 1s signal becomes significantly less when the reduction potential increases from -0.4 to -0.6 V (Figure S15). Combining this with the above electrocatalytic performance results, we suppose the C=O group is the active site for NRR activity on GO. In addition, Raman and FTIR spectra are collected for further vibration information analysis. In Figure 3e, the peaks at 1320 and 1590 cm^{-1} belong to the characteristic D band and G band of carbon materials, representing the defects of carbon lattice atoms and the plane vibration of ordered graphite structure, respectively.³³ The I_D/I_G ratios for ERGO-0.4 and ERGO-0.6 are 1.31 to 1.26, revealing more oxygen species are reduced under a higher reducing potential. They are both substantially larger than pure GO nanosheets (Figure S16), indicating the decrease in size of the in-plane sp^2 domains.³¹ Fourier transform infrared (FTIR) spectra confirm that the majority of the C=O groups located at 1796 cm^{-1} are reduced (Figure 3f).^{34,35} These are consistent with the above XPS discussions.

Density functional theory (DFT) calculations are further performed to identify the potential of individual oxygen species for NRR and to understand the underlying reaction mechanism. As the first starting step, efficient molecular N₂ fixation and activation are the prerequisites for following the ammonia synthesis pathway. A variety of N₂ adsorption configurations on the graphene-based substrates is constructed. After optimization, it is found the N₂ molecule is far from the pristine graphene surface with the distance larger than 3 Å. The similar phenomenon is observed on the graphene sheets with OH and O–C–O modifications, manifesting that the N₂ molecules cannot be adsorbed on a graphene surface with these oxygenated group modifications (Figure S17). In contrast, Figure 4a shows the C=O group on graphene can interact with N₂ tightly, with the two N atoms combining with the C and O atoms, respectively, in the side-on adsorption configuration. The average distance between the N₂ and C=O groups is 1.45 Å, indicating a strong adsorption at the interface. Figure 4b suggests the N≡N bond length is elongated from 1.10 Å of free N₂ molecular to 1.24 Å in the adsorbed case, accompanied by the C=O bond length increasing from 1.22 to 1.46 Å.

Meanwhile, the vibration frequency of the C=O bond decreases from 1769.4 to 1768.9 cm^{-1} after the N₂ adsorption. Besides, the charge density difference (CDD) calculation shown in Figure 4c presents a two-way charge transfer process for the adsorption with charge accumulation and depletion simultaneously occurring on the adsorbed N₂ molecule. This phenomenon is in accordance with the “acceptance-donation” electron reservoir for NRR as described before.³⁶ Figure 4d shows the corresponding projected density of states (PDOS) calculation, in which the C=O group provides more hybridization with N₂. These are consistent with our experimental observations, illustrating that C=O plays a critical role for N₂ fixation and activation. It is noted that the COOH group also contains the C=O counterpart, and Figure S18 shows COOH can also combine with N₂ strongly, further

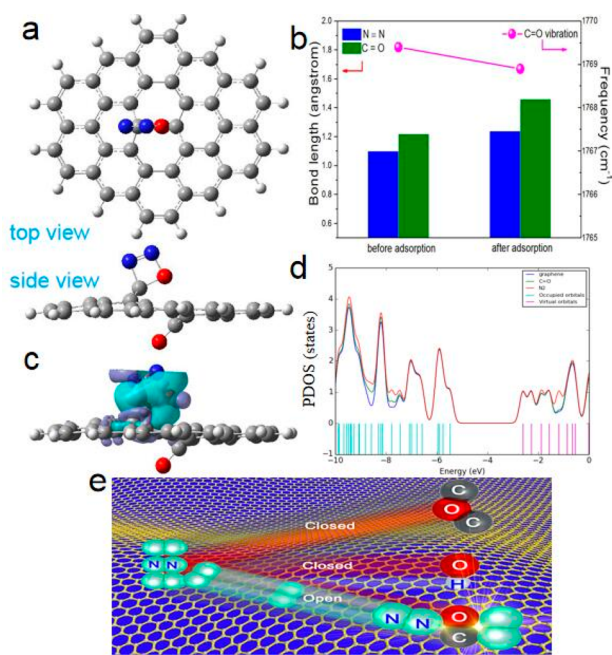


Figure 4. DFT calculations for the N₂ adsorption on C=O decorated graphene. (a) The optimized structure, with gray, red, blue, and white balls representing C, O, N, and H atoms, respectively. (b) The N≡N bond lengths, C=O bond lengths, and C=O vibration frequencies before and after N₂ adsorption. (c) CDD at the interface, with purple and green standing for positive and negative charge distributions, respectively. (d) PDOS for the complex. (e) Schematic illustration for N₂ fixation on different oxygenated groups.

strengthening the efficiency of C=O for N₂ adsorption and activation. All of these discussions and N₂ adsorption cases are schematically illustrated in Figure 4e. In addition, we find the NH₂ intermediate is loosely adsorbed with C=O decorated graphene (+0.13 eV), which can facilitate the NH₃ release and guarantee the NRR process proceeding forward (Figure S19).³⁷ In the meantime, the H atom demonstrates an inefficient adsorption, implying a low activity for hydrogen evolution, consisting of the high FE efficiency.

In summary, GO has been demonstrated as an efficient metal-free catalyst to be used in the hydrogenation of N₂ to NH₃ under ambient conditions. In situ electroreduction is employed to controllably reduce the oxygenated groups on surface. Combining the experimental observations and the DFT calculations, the C=O group is found to play a critical role for the N₂ molecule fixation following the acceptance-donation mechanism. Meanwhile, the C=O group affords a weak adsorption for the NH₂ intermediate. These are conducive to N₂ activation and to the NRR proceeding. We hope this study can provide new guidance for the rational design and further development of carbon-based materials.

■ ASSOCIATED CONTENT

SI Supporting Information

The Supporting Information is available free of charge at <https://pubs.acs.org/doi/10.1021/acs.inorgchem.0c01596>.

Experiments, UV–vis absorption spectra, DFT calculations, and comparisons (PDF)

■ AUTHOR INFORMATION

Corresponding Authors

Xiangkai Kong – Key Laboratory of Green and Precise Synthetic Chemistry and Application, Ministry of Education & Anhui Province Key Laboratory of Pollutant Sensitive Materials and Environmental Remediation, Huaibei Normal University, Huaibei 235000, Anhui, P. R. China; Key Laboratory of Structure and Functional Regulation of Hybrid Materials, Anhui University, Hefei 230601, P. R. China; orcid.org/0000-0002-0552-5557; Email: kxk@chnu.edu.cn

Guilin Chen – College of Physics and Energy, Fujian Normal University, Fuzhou 350007, Fujian, P. R. China; orcid.org/0000-0003-3535-8240; Email: glchen@fjnu.edu.cn

Authors

Sini Wang – Key Laboratory of Green and Precise Synthetic Chemistry and Application, Ministry of Education & Anhui Province Key Laboratory of Pollutant Sensitive Materials and Environmental Remediation, Huaibei Normal University, Huaibei 235000, Anhui, P. R. China

Jingjing Zhu – Key Laboratory of Green and Precise Synthetic Chemistry and Application, Ministry of Education & Anhui Province Key Laboratory of Pollutant Sensitive Materials and Environmental Remediation, Huaibei Normal University, Huaibei 235000, Anhui, P. R. China

Yicheng Zhang – Key Laboratory of Green and Precise Synthetic Chemistry and Application, Ministry of Education & Anhui Province Key Laboratory of Pollutant Sensitive Materials and Environmental Remediation, Huaibei Normal University, Huaibei 235000, Anhui, P. R. China

Qiangchun Liu – Key Laboratory of Green and Precise Synthetic Chemistry and Application, Ministry of Education & Anhui Province Key Laboratory of Pollutant Sensitive Materials and Environmental Remediation, Huaibei Normal University, Huaibei 235000, Anhui, P. R. China

Complete contact information is available at:

<https://pubs.acs.org/10.1021/acs.inorgchem.0c01596>

Notes

The authors declare no competing financial interest.

■ ACKNOWLEDGMENTS

This work is supported by the National Natural Science Foundation of China (51602116), the Natural Science Foundation of Anhui Province (1708085QB40, to X.K.), and the Open Project of Key Laboratory of Structure and Functional Regulation of Hybrid Materials (Anhui University), Ministry of Education. The calculations have been completed on the Supercomputing system in the Supercomputing Center of USTC.

■ REFERENCES

- (1) Tang, C.; Qiao, S. Z. How to explore ambient electrocatalytic nitrogen reduction reliably and insightfully. *Chem. Soc. Rev.* **2019**, *48*, 3166–3180.
- (2) Li, L.; Tang, C.; Xia, B.; Jin, H.; Zheng, Y.; Qiao, S. Z. 2D Mosaic Bismuth Nanosheets for Highly Selective Ambient Electrocatalytic Nitrogen Reduction. *ACS Catal.* **2019**, *9*, 2902–2908.
- (3) Suryanto, B. H. R.; Du, H. L.; Wang, D.; Chen, J.; Simonov, A. N.; MacFarlane, D. R. Challenges and prospects in the catalysis of electroreduction of nitrogen to ammonia. *Nat. Catal.* **2019**, *2*, 290–296.

- (4) Zhao, R.; Xie, H.; Chang, L.; Zhang, X.; Zhu, X.; Tong, X.; Wang, T.; Luo, Y.; Wei, P.; Wang, Z.; Sun, X. Recent progress in the electrochemical ammonia synthesis under ambient conditions. *EnergyChem*. **2019**, *1*, 100011.
- (5) Guo, J. C.; Wang, H.; Xue, F.; Yu, D.; Zhang, L.; Jiao, S. L.; Liu, Y. H.; Lu, Y. F.; Liu, M. C.; Ruan, S. C.; Zeng, Y. J.; Ma, C.; Huang, H. W. Tunable synthesis of multiply twinned intermetallic Pd₃Pb nanowire networks toward efficient N₂ to NH₃ conversion. *J. Mater. Chem. A* **2019**, *7*, 20247–20253.
- (6) Davy, H. On Some Chemical Agencies of Electricity London, Lecture. *Trans. R. Soc.* **1807**, *97*, 1.
- (7) Zhao, Y.; Shi, R.; Bian, X.; Zhou, C.; Zhao, Y.; Zhang, S.; Wu, F.; Waterhouse, G. I. N.; Wu, L. Z.; Tung, C. H.; Zhang, T. Ammonia Detection Methods in Photocatalytic and Electrocatalytic Experiments: How to Improve the Reliability of NH₃ Production Rates? *Adv. Sci.* **2019**, *6*, 1802109.
- (8) Geng, Z.; Liu, Y.; Kong, X.; Li, P.; Li, K.; Liu, Z.; Du, J.; Shu, M.; Si, R.; Zeng, J. Achieving a Record-High Yield Rate of 120.9 for N₂ Electrochemical Reduction over Ru Single-Atom Catalysts. *Adv. Mater.* **2018**, *30*, 1803498.
- (9) Tao, H.; Choi, C.; Ding, L. X.; Jiang, Z.; Han, Z.; Jia, M.; Fan, Q.; Gao, Y.; Wang, H.; Robertson, A. W.; Hong, S.; Jung, Y.; Liu, S.; Sun, Z. Nitrogen fixation by Ru single-atom electrocatalytic reduction. *Chem.* **2019**, *5*, 204–214.
- (10) Bao, D.; Zhang, Q.; Meng, F. L.; Zhong, H. X.; Shi, M. M.; Zhang, Y.; Yan, J. M.; Jiang, Q.; Zhang, X. B. Electrochemical Reduction of N₂ under Ambient Conditions for Artificial N₂ Fixation and Renewable Energy Storage Using N₂/NH₃ Cycle. *Adv. Mater.* **2017**, *29*, 1604799.
- (11) Zhang, J.; Ji, Y.; Wang, P.; Shao, Q.; Li, Y.; Huang, X. Adsorbing and Activating N₂ on Heterogeneous Au–Fe₃O₄ Nanoparticles for N₂ Fixation. *Adv. Funct. Mater.* **2020**, *30*, 1906579.
- (12) Wang, J.; Yu, L.; Hu, L.; Chen, G.; Xin, H.; Feng, X. Ambient ammonia synthesis via palladium-catalyzed electrohydrogenation of dinitrogen at low overpotential. *Nat. Commun.* **2018**, *9*, 1795.
- (13) Hui, L.; Xue, Y.; Yu, H.; Liu, Y.; Fang, Y.; Xing, C.; Huang, B.; Li, Y. Highly efficient and selective generation of ammonia and hydrogen on a graphdiyne-based catalyst. *J. Am. Chem. Soc.* **2019**, *141*, 10677–10683.
- (14) Zeng, L.; Chen, S.; Van der Zalm, J.; Li, X.; Chen, A. Sulfur vacancy-rich N-doped MoS₂ nanoflowers for highly boosting electrocatalytic N₂ fixation to NH₃ under ambient conditions. *Chem. Commun.* **2019**, *55*, 7386–7389.
- (15) Zhu, X.; Liu, Z.; Wang, H.; Zhao, R.; Chen, H.; Wang, T.; Wang, F.; Luo, Y.; Wu, Y.; Sun, X. Boosting electrocatalytic N₂ reduction to NH₃ on β-FeOOH by fluorine doping. *Chem. Commun.* **2019**, *55*, 3987–3990.
- (16) Xia, L.; Li, B.; Zhang, Y.; Zhang, R.; Ji, L.; Chen, H.; Cui, G.; Zheng, H.; Sun, X.; Xie, F.; Liu, Q. Cr₂O₃ Nanoparticle-Reduced Graphene Oxide Hybrid: A Highly Active Electrocatalyst for N₂ Reduction at Ambient Conditions. *Inorg. Chem.* **2019**, *58*, 2257–2260.
- (17) Qiu, W.; Xie, X. Y.; Qiu, J.; Fang, W. H.; Liang, R.; Ren, X.; Ji, X.; Cui, G.; Asiri, A. M.; Cui, G.; Tang, B.; Sun, X. High-performance artificial nitrogen fixation at ambient conditions using a metal-free electrocatalyst. *Nat. Commun.* **2018**, *9*, 3485.
- (18) Zhang, X.; Wu, T.; Wang, H.; Zhao, R.; Chen, H.; Wang, T.; Wei, P.; Luo, Y.; Zhang, Y.; Sun, X. Boron Nanosheet: An Elemental Two-Dimensional (2D) Material for Ambient Electrocatalytic N₂-to-NH₃ Fixation in Neutral Media. *ACS Catal.* **2019**, *9*, 4609–4615.
- (19) Zhang, L.; Ding, L. X.; Chen, G. F.; Yang, X.; Wang, H. Ammonia synthesis under ambient conditions: Selective electroreduction of dinitrogen to ammonia on black phosphorus nanosheets. *Angew. Chem., Int. Ed.* **2019**, *58*, 2612–2616.
- (20) Chen, C.; Yan, D.; Wang, Y.; Zhou, Y.; Zou, Y.; Li, Y.; Wang, S. B-N Pairs Enriched Defective Carbon Nanosheets for Ammonia Synthesis with High Efficiency. *Small* **2019**, *15*, 1805029.
- (21) Huang, C.; Li, Y.; Wang, N.; Xue, Z.; Liu, H.; Li, Y.; Zuo, Z. Progress in research into 2D Graphdiyne-Based Materials. *Chem. Rev.* **2018**, *118*, 7744–7803.
- (22) Li, Q.; Zhu, J.; Wang, S.; Huang, F.; Liu, Q.; Kong, X. Microwave absorption on a bare biomass derived holey silica-hybridized carbon absorbent. *Carbon* **2020**, *161*, 639–646.
- (23) Xue, Y.; Huang, B.; Yi, Y.; Guo, Y.; Zuo, Z.; Li, Y.; Jia, Z.; Liu, H.; Li, Y. Anchoring zero valence single atoms of nickel and iron on graphdiyne for hydrogen evolution. *Nat. Commun.* **2018**, *9*, 1460.
- (24) Jia, Z.; Li, Y.; Zuo, Z.; Liu, H.; Huang, C.; Li, Y. Synthesis and properties of 2D Carbon-Graphdiyne. *Acc. Chem. Res.* **2017**, *50*, 2470–2478.
- (25) Li, Y.; Xu, L.; Liu, H.; Li, Y. Graphdiyne and graphyne: from theoretical predictions to practical construction. *Chem. Soc. Rev.* **2014**, *43*, 2572.
- (26) Wang, T.; Xia, L.; Yang, J.; Wang, H.; Fang, W.; Chen, H.; Tang, D.; Asiri, A.; Luo, Y.; Cui, G. L.; Sun, X. Electrocatalytic N₂-to-NH₃ conversion using oxygen-doped graphene: experimental and theoretical studies. *Chem. Commun.* **2019**, *55*, 7502.
- (27) Yu, X.; Han, P.; Wei, Z.; Huang, L.; Gu, Z.; Peng, S.; Ma, J.; Zheng, G. Boron-doped graphene for electrocatalytic N₂ reduction. *Joule*. **2018**, *2*, 1610–1622.
- (28) Zhao, J.; Yang, J.; Ji, L.; Wang, H.; Chen, H.; Niu, Z.; Liu, Q.; Li, T.; Cui, G.; Sun, X. Defect-rich fluorographene nanosheets for artificial N₂ fixation under ambient conditions. *Chem. Commun.* **2019**, *55*, 4266–4269.
- (29) Chen, H.; Zhu, X.; Huang, H.; Wang, H.; Wang, T.; Zhao, R.; Zheng, H.; Asiri, A. M.; Luo, Y.; Sun, X. Sulfur dots-graphene nanohybrid: a metal-free electrocatalyst for efficient N₂-to-NH₃ fixation under ambient conditions. *Chem. Commun.* **2019**, *55*, 3152–3155.
- (30) Liu, Q.; Wang, S.; Chen, G.; Liu, Q.; Kong, X. Activating Graphyne Nanosheet via sp-Hybridized Boron Modulation for Electrochemical Nitrogen Fixation. *Inorg. Chem.* **2019**, *58*, 11843–11849.
- (31) Guo, H. L.; Wang, X. F.; Qian, Q. Y.; Wang, F. B.; Xia, X. H. A green approach to the synthesis of graphene nanosheets. *ACS Nano* **2009**, *3*, 2653–2659.
- (32) Al-Gaashani, R.; Najjar, A.; Zakaria, Y.; Mansour, S.; Atieh, M. A. XPS and structural studies of high quality graphene oxide and reduced graphene oxide prepared by different chemical oxidation methods. *Ceram. Int.* **2019**, *45*, 14439–14448.
- (33) Wang, S.; Hu, K.; Huang, F.; Zhang, M.; Wu, S.; Liu, Q.; Kong, X. Activating microwave absorption via noncovalent interaction at interface based on metal-free graphene nanosheets. *Carbon* **2019**, *152*, 818–826.
- (34) Kong, X.; Chen, Q.; Lun, Z. Probing the influence of different oxygenated groups on graphene oxide's catalytic performance. *J. Mater. Chem. A* **2014**, *2*, 610–613.
- (35) Zhang, X.; Feng, Y.; Huang, D.; Li, Y.; Feng, W. Investigation of optical modulated conductance effects based on a graphene oxide-azobenzene hybrid. *Carbon* **2010**, *48*, 3236–3241.
- (36) Ling, C.; Niu, X.; Li, Q.; Du, A.; Wang, J. Metal-Free Single Atom Catalyst for N₂ Fixation Driven by Visible Light. *J. Am. Chem. Soc.* **2018**, *140*, 14161–14168.
- (37) Zhao, J.; Chen, Z. Single Mo atom supported on defective boron nitride monolayer as an efficient electrocatalyst for nitrogen fixation: a computational study. *J. Am. Chem. Soc.* **2017**, *139*, 12480–12487.